Liquid-core-microtubule-enhanced Laser sensor for high resolution temperature measurement

Yize Liu, Junfeng Jiang, Kun Liu, Shuang Wang, Panpan Niu, Danni Jiao, Tianhua Xu, Xuezhi Zhang, and Tiegen Liu

***Abstract*—We present a fiber laser temperature sensor based on temperature dependence whisper gallery mode-based microcavity. Three different thermo-optic coefficient liquids are injected into a thin wall thickness microtubule for different temperature sensitivity of whisper gallery mode shift. The sensor temperature sensitivity increases with the absolute value of the liquid core thermo-optic coefficient. The theoretical model of whisper gallery mode temperature response is analyzed. A liquid core microtubule is inserted into the erbium-doped fiber ring laser cavity as the optical filter and sensing unit simultaneously, so the lasing wavelength can be used to detect the temperature change of the medium. Due to the narrow spectral width of sensing laser, a high sensing resolution system is experimentally confirmed. With the combination of liquid core to increase the sensitivity and fiber ring laser cavity to increase sensing resolution, the high sensitivity 112.8 pm/°C of sensing system is demonstrated and the thermal resolution is 8.16 × 10^{-3} °C.**

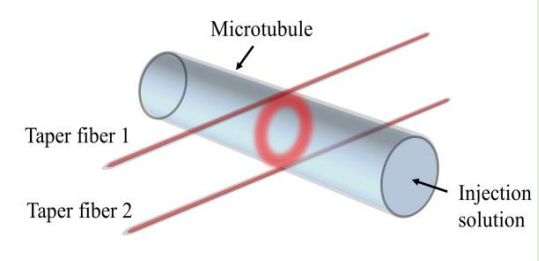

***Index Terms*—Whisper gallery mode, fiber optics sensors, temperature measurement**

I. Introduction

Whispering gallery mode (WGM) resonators are usually azimuthally symmetric structures in the range from tens to hundreds of μm and have been successfully demonstrated in various geometries including microbubbles (microspheres), microrings and microtoroids [1-5]. They can restrict light internally by the continuous total internal reflection process, which means confining resonant photons in the microscale volume for long periods of time. Consequently, this characteristic strongly enhances the light-matter interaction. Due to the features of high quality (Q)-factor and small modal volume, they become promising platforms for precise sensing, such as pressure [6], strain [7], biology [8, 9] and temperature [10-14]. Specifically, in temperature sensing, most commonly used method is WGMs shift detecting. The environmental temperature perturbations can be reflected in the changes of WGMs resonant wavelength due to the thermo-optic (temperature dependence of the material refractive index) and thermal expansion (change of the resonator size) effects.

In early temperature sensing systems, solid silica microbubble is used as the resonator and the temperature coefficient of the WGMs is constant ~6ppm [15]. A larger thermo-optic coefficient and/or thermal expansion coefficient typically leads to a larger frequency shift and thus numerous devices have been proposed. The organic resonators are chosen duo to the large thermal expansion coefficient [14, 16]. However, organic materials, especially polydimethylsiloxane (PDMS) show a slower response (more than hundred seconds) due to poor thermal conductivity. In addition, the consistency between heating and cooling cycle is worse due to the large hysteresis essence [17]. So, despite its potential sensitivity and resolution, there are limitations in actual sensing. Another candidate is liquid resonators (dye-doped oil [11, 18], liquid crystal [19]), benefit from its improvement in both coefficients. Although the sensing sensitivity is greatly enhanced, the excited lasing in the liquid droplet will reduce the resolution. In order to overcome the short life time, they are usually used in a water solution. On the other hand, the thin wall thickness hollow cavity can be filled with high thermo-optic coefficient liquid to enhance the temperature sensitivity. However, the liquid-core resonators reduce the Q value and does not significantly improve the resolution. Overall, previous works mainly focus on the optimization of sensitivity, and ignore the balance of sensitivity and resolution.

This work was supported by National Natural Science Foundation of China (Grant No. 61735011, U2006216); National Instrumentation Program of China (Grant No. 2022YFF0706000); and the open project of Key Laboratory of Opto-electronics Information Technology (Grant No. 2022KFKT004, 2022KFKT005); the open project of Key Laboratory of Micro Opto-electro Mechanical System Technology (Grant No. 2022KFKT006). (Corresponding authors: Junfeng Jiang.)

The authors are with the School of Precision Instruments and Opto-Electronics Engineering, and Tianjin Optical Fiber Sensing Engineering Center, Institute of Optical Fiber Sensing, China, and Key Laboratory of Opto-electronics Information Technology, Tianjin University, Tianjin 300072, China. T. Xu is also with the School of Engineering, University of Warwick, Coventry, United Kingdom CV47AL. (e-mail: liu_yize@tju.edu.cn; jiangjfjxu@tju.edu.cn; beiyangkl@tju.edu.cn; shuangwang@tju.edu.cn; niupanpan@tju.edu.cn; jiaodanni@tju.edu.cn; xutianhua@tju.edu.cn; zhangxz@tju.edu.cn; tgliu@tju.edu.cn).

In this work, we demonstrated a fiber ring laser (FRL) enhanced temperature sensor based on a liquid-core microtubule WGM resonator. With high thermo-optic coefficient liquid injection, the WGM temperature sensitivity of hollow microtubule which is fabricated with pressurized tapering technology is increased. In addition, the dual-fiber coupled microtubule is used as a filter in fiber ring laser system to adjust the output wavelength. Therefore, the resulting temperature dependent sensing laser with narrow spectral width can greatly improve the temperature resolution. By the combination of the two methods, the temperature changes can be evaluated by recording the spectrum evolution of the sensing laser, and a maximum temperature sensitivity up to 112.8 pm/°C, temperature resolution of 8.16 × 10^{-3} °C are achieved.

II. PRINCIPLE

A. The fabrication of microtubule cavity and taper fibers

The wall-thickness-controlled microtubules are fabricated from commercial fused silica capillary (TSP250350, Polymicro Inc.) by fused tapering process with inner pressurized air. Through the control of applied pressure and elongated length, a pressurized microcapillary tapering model is established to control the wall thickness and radius. Therefore, ultra-thin (typical value: ~1.5 μm) silica microtubule WGM resonator with large radius (typical value: ~35 μm) can be fabricated. More details can refer in our previous work [20]. The ultra-thin wall thickness structure can distribute more electric field energy in the microcavity core and thus obtain higher sensing sensitivity. The adiabatic tapered fibers are fabricated by using flame resweep method [21]. The typical waist diameter of taper fiber is 3 μm. Smaller waist diameter taper fiber can couple to higher radial modes of WGM and increasing temperature sensitivity correspondingly [22].

B. Liquid-core microtubule WGM and its temperature response characteristic

The microtubule cavity can support WGM resonance, and its resonant mode can be expressed as

$$2\pi n_{\mathrm{eff}} R_1 = m\lambda_m \tag{1}$$

where R_1 is the microtubule outer radius, n_{eff} is the corresponding effective refractive index, m is a positive integer representing the number of WGM angular modes. λ is the WGM resonant wavelength. The temperature induced WGM wavelength shift $d\lambda$ in a hollow microtubule can be expressed as [11, 13]

$$\frac{d\lambda}{\lambda} = \alpha dT + \frac{\partial n_{eff}}{\partial T}\frac{1}{n_{eff}}dT \tag{2}$$

the first term represents material thermal expansion coefficient, $\alpha = \frac{\partial R_1}{\partial T}\frac{1}{R_1}$. The second term is thermo-optic coefficient, and the effective refractive index change rate is

$$\frac{\partial n_{eff}}{\partial T} = k_{core}\frac{\partial n_{eff}}{\partial n_{core}} + k_{wall}\frac{\partial n_{eff}}{\partial n_{wall}} + k_{air}\frac{\partial n_{eff}}{\partial n_{air}} + \alpha_{wall}\frac{\partial n_{eff}}{\partial t} \tag{3}$$

where n_{core}, n_{wall} and n_{air} are the refractive indices of liquid core inside cavity, silica wall and air outside cavity, respectively. k_{core}, k_{wall} and k_{air} are their thermo-optic coefficients, respectively. t is the wall thickness. Since k_{air} and α_{wall} are relatively small, the last two terms can be ignored. Finally, the resonance wavelength temperature sensitivity can be obtained as

$$S_T = \frac{d\lambda}{dT} = \lambda(\alpha + \frac{k_{core}}{n_{eff}}\frac{\partial n_{eff}}{\partial n_{core}} + \frac{k_{wall}}{n_{eff}}\frac{\partial n_{eff}}{\partial n_{wall}}) \tag{4}$$

where $\alpha = 5\times10^{-7}\,℃^{-1}$, $k_{wall} = 11\times10^{-7}\,℃^{-1}$, $n_{wall} = 1.45$ for silica material. k_{core} and n_{core} are related to the injection solution.

In order to numerically describe the temperature sensitivity, the electric field distribution of the double-fiber-coupled microtubule with cyclohexane core $k_{core}^{c} = -5.4\times10^{-4}\,℃^{-1}$, $n_{\mathrm{core}}^{c} = 1.4262$ is simulated as an example. The WGM spectrum measurement system with the apparatuses is illustrated in Fig. 1(a). Two coupled taper fibers are arranged orthogonally along the axial direction of the microtubule, one of which is used to excite the WGM and the other is used to collect the signal after circumferential transmission in microtubule. The hollow microtubule is filled with cyclohexane by a syringe. The optical microscopic image of the microtubule with outer radius R_1=32.48 μm is shown in Fig. 1 (a) inset. The light from a computer controlled tunable laser (TL, Keysight 81607 A, linewidth: <10 kHz, tunable range: 1500~1600 nm) is coupled into the microtubule through the first lower tapered fiber. After exciting the WGM, the lower tapered fiber port 2 and second upper tapered fiber port 3 are connected to the optical switch (OS). The total output is connected to a powermeter module (PM, Keysight 81636B) to collect and display the transmission (Port2) or reflection (Port3) WGM spectrum in real time, as shown in Fig. 1(b). It can be seen that the transmission and reflection spectra have the same resonant period, but the opposite spectral pattern. The Q-factor (defined as $Q=\lambda/\Delta\lambda$, where $\Delta\lambda$ is the linewidth of the peak) of the resonance around 1528.7 nm in transmission spectrum Q_t=1.1×10^4, in reflection spectrum Q_r=8.1×10^3. A polarization controller (PC) could adjust the WGM polarization state. According to theoretical calculations based on characteristic equations of optical modes [23, 24], the experimental WGMs are well-fitted with the theoretical first radial order (angular mode number from 181 to 184) TM polarization modes, as shown in Fig. 1(b) inset. The radial dependent electric field can be expressed by Bessel function in the following form [25]

$$E_z(r) = \begin{cases} AJ_m(\kappa n_{core}R)\cdots R \le R_2 \\ BJ_m(\kappa n_{wall}R) + CN_m(\kappa n_{wall}R)\cdots R_2 < R \le R_1 \\ DH_m^{(1)}(\kappa n_{air}R)\cdots R > R_1 \end{cases} \tag{5}$$

where κ is the vacuum wave-vector, and R_2 is the internal radius of microtubule, J_m, N_m, $H_m^{(1)}$ are the m order cylindrical

Bessel function, Neumann function and Hankel function of the first kind, respectively. Through boundary conditions, the radial dependent electric field of TM_{183}^{1} (the radial mode number=1, the angular mode number m=183) is shown in Fig. 2. When the typical 1.5 μm wall thickness is chosen, the electric field distributed in the core, wall, and air are $\eta_1 = 18.5\%$, $\eta_2 = 81.3\%$ and $\eta_3 = 0.2\%$, respectively. Since the effective refractive index is determined by the electric field distribution, the theoretical sensitivity is 105.37 pm/°C according to Eq. (4).

C. WGM microtubule intra-cavity fiber ring laser temperature sensor

Due to the comb spectrum of WGM, the microtubule cavity with spatial filtering characteristics can be considered as a high-contrast optical filter to realize the wavelength selecting function. Meanwhile, the spatial filtering characteristics of the microtubule can respond to the WGM resonance wavelength drift with the temperature change. Therefore, the sensing laser for temperature can be realized by inserting the microtubule into the FRL cavity, which will have the advantage of high optical power and narrow spectral width.

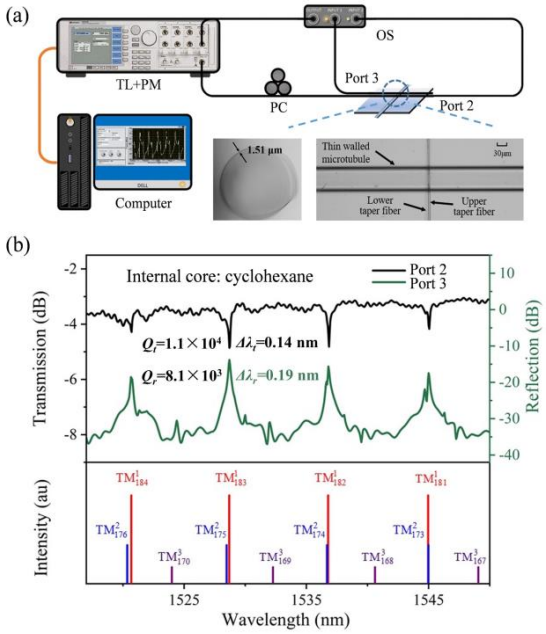

Fig. 1. (a) Experimental setup of the WGM spectrum measurement system. Inset: optical microscopic images of the microtubule cross section and double-fiber-coupled region. (b) Transmission (Port2) and reflection (Port3) WGM spectra of the double-fiber-coupled microtubule cavity. Inset: theoretical first-order TM polarization modes from 181 to 184, the second-order TM polarization modes from 173 to 176 and the third-order TM polarization modes from 167 to 170.

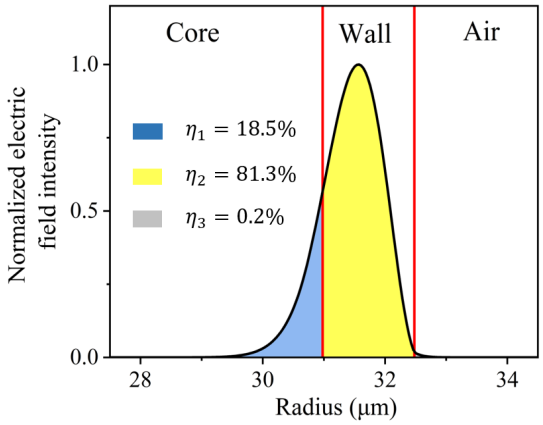

Fig. 2. Normalized electric field intensity distribution in radial direction of the microtubule.

The FRL temperature sensing system based on WGM is proposed in Fig. 3(a). The system is formed by two taper fibers, a 1 m erbium-doped fiber (EDF, Er80-4/125, Liekki) and a microtubule cavity. The 980 nm laser is injected into the system through a 980/1550 nm wavelength division multiplexer (WDM). The light enters microtubule from port 1 of taper fiber 1, and part of the light is coupled into the cavity through evanescent field in the coupling point 1. After circumferential propagation, the light is coupled out from port 3 of taper fiber 2. The microtubule and two taper fibers constitute the sensing unit and a cross-sectional diagram is shown in Fig. 3(b). An optical isolator (ISO) ensured the unidirectional propagation of light in the FRL, and a polarization controller (PC) could adjust the polarization state. When the high-quality spatial filtering properties microtubule is presented in a ring cavity with saturated EDF, the corresponding resonance peak obtains cyclic cumulative gain and is amplified. Therefore, the ring cavity can generate a single-wavelength laser with relative narrow full width at half maxima (FWHM) for temperature sensing. The output sensing laser is extracted by a 5:95 optical coupler (OC), and recorded by an optical spectrum analyzer (OSA, AQ6370, Yokogawa).

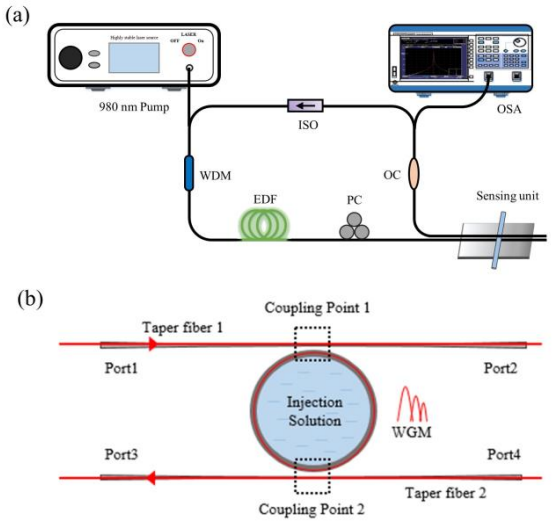

Fig. 3. (a) Experiment setup of the proposed fiber laser temperature sensor. (b) Cross sectional diagram for the sensing unit.

III. RESULTS

A. Temperature response of WGM sensing unit

To characterize the temperature response of the WGM, the microtubule is placed on a controlled temperature platform to experience different temperatures in WGM spectrum measurement system. The microtubule is full filled with liquid and sealed one side by UV glue. Furthermore, we can change the temperature sensitivity by injecting different liquid core. The sensitivity is proportional to the absolute value of the injected liquid thermo-optical coefficient. Three different solutions, cyclohexane, ethanol and acetone are individually injected into the hollow microtubule for temperature sensing experiments. The thermo-optic coefficient of ethanol and acetone are $k^{e}_{core} = -3.9\times10^{-4}℃^{-1}$ and $k^{a}_{core} = -5.0\times10^{-4}℃^{-1}$. We pump deionized water into the hollow microtubule several times before injecting different solutions. When the temperature controlled from 20 °C to 24 °C, the WGM temperature response of port 3 near 1530 nm are shown in Figs. 4(a)–(c). We hope to use the microtubule-based sensors in the field of upper mixed layer (0-200 meters) ocean temperature sensing in the future. This range include moderate temperature of upper mixed layer ocean. In addition, the FRL system with microtubule covering the whole temperature range in upper mixed layer ocean applications is demonstrated in the following part. With the increase of temperature, the WGM reflection spectrum has a blueshift, and the linear fitting shows a temperature sensitivity of 64.1 pm/°C, 95.6 pm/°C and 114.5 pm/°C when the core of the microtubule is ethanol, acetone and cyclohexane, respectively. The experimental results show the same shorter wavelength drift with the theoretical analysis. In additional, the numerical simulation sensitivity 105.37 pm/°C of cyclohexane is approximately equal to the experimental data.

B. Temperature sensor based on FRL system with WGM microtubule

In the experiment, the cyclohexane core microtubule with highest sensitivity is coupled in the FRL system to induce the temperature sensing laser at the resonant wavelength at about 1528.7 nm (TM^{1}_{183}), as shown in Fig. 5 (blue line). The single wavelength lasing output is realized by adjusting the polarization dependent loss of ring cavity with the polarization controller. To achieve a more stable single wavelength laser output, we can reduce the microtubule radius to increase the resonant peak free spectrum range or use a bandpass filter. Fig. 5 (green line) shows the forward-pump amplified spontaneous emission (ASE) spectrum of the FRL, which has typical EDF-based ASE spectral characteristics. The original reflection from the port 3 is shown in Fig. 5 (red line). Compared with reflection spectrum, the single wavelength lasing oscillation at 1528.7 nm has narrower FWHM of 0.015 nm and higher optical signal-to-noise ratio of 52 dB, as shown in the insets of Fig. 5. Thus, the resolution of sensing system is improved by an order of magnitude. It should be noted that the measured FWHM of sensing laser is limited by the wavelength resolution of the OSA and a smaller FWHM close to the true value can be obtained by the other subsequent methods, such as delayed self-heterodyne technique with Voigt profile fitting [26]. In our experiment, the OSA is directly used to monitor sensing laser wavelength change because of its convenience.

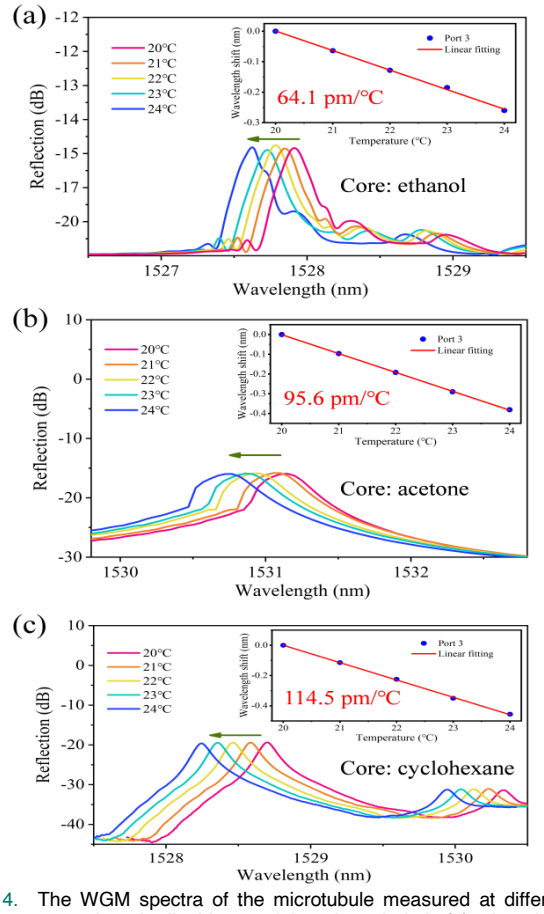

Fig. 4. The WGM spectra of the microtubule measured at different temperatures when the liquid core of the microtubule is (a) ethanol, (b) acetone, and (c) cyclohexane. Insets: temperature sensitivities of three different liquids.

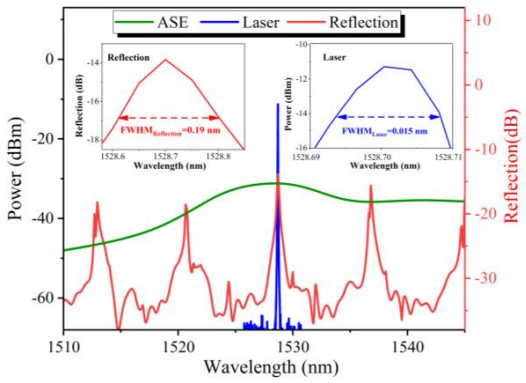

Fig. 5. Forward-pump ASE, output sensing laser spectra of the FRL, and reflection WGM spectrum of the microtubule cavity. Insets: enlarged views of the peaks in the sensing laser and the original reflection spectrum.

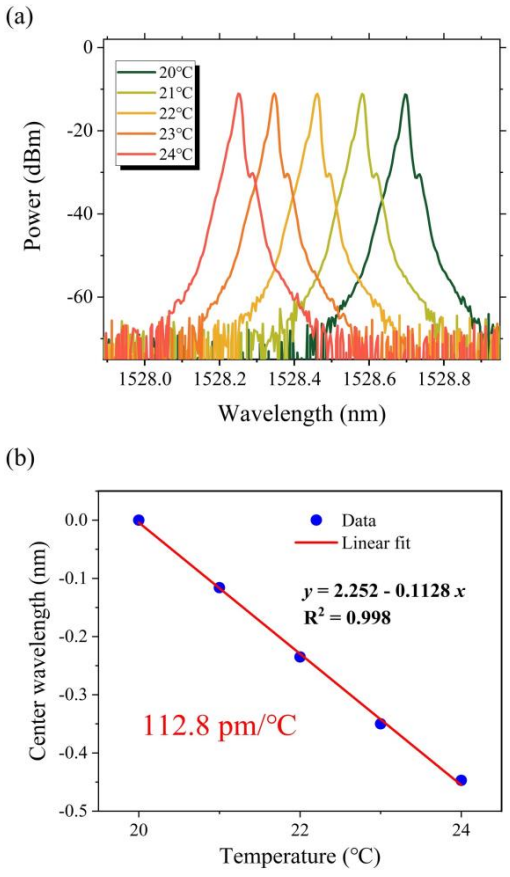

Fig. 6. (a) The output sensing laser at different temperatures. (b) The temperature sensitivity of the sensing system.

In the temperature measurement, the sensing laser is pumped and the sensing unit microtubule is also placed on the controlled temperature platform to experience different temperatures. The temperature is increased from 20 ℃ to 24 ℃ with a step of 1 ℃, the sensing laser spectral evolutions are shown in Fig. 6. The result shows that the sensing laser of the FRL has a blue shift as the temperature increases and the temperature sensitivity is 112.8 pm/℃. As previously described, the wavelength shift of the output sensing laser is determined by the temperature characteristics of the WGM microtubule. So, the peak wavelength of sensing laser has the same temperature shift direction with WGM reflection spectrum temperature response in Fig. 4 and the two temperature sensitivities are almost equal. For ethanol and acetone core, the trends are the same. To demonstrate the resolution of our sensor, the temperature of the cyclohexane liquid core sensing laser is increased from 20 ℃ to 20.4 ℃, with a step of 0.05 ℃. Each temperature sample is measured ten times with an interval of 15 seconds. The output laser spectra are recorded by OSA and the center wavelength is obtained by Lorentz fitting. The measured temperatures with time are calculated from center wavelength and shown in Fig. 7(a). The difference and the standard deviation between measurement mean temperatures and controlled temperatures are shown in Fig. 7(b). The temperature resolution of sensors can be considered as the mean standard deviation of each temperature sample in Fig. 7(b). So, the temperature resolution is 8.16×10^{-3} ℃ accordingly.

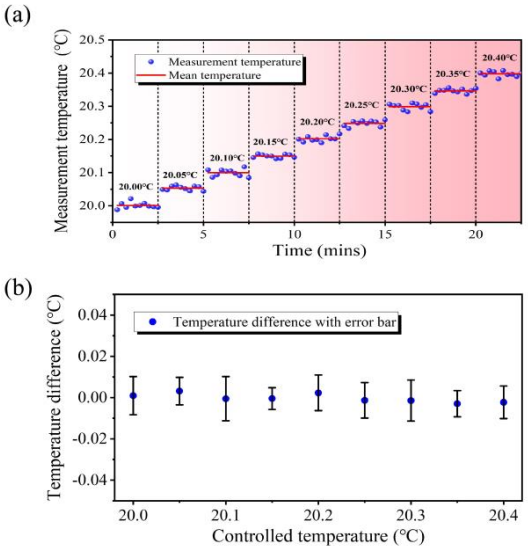

Fig. 7. (a) Measured temperatures changing with time. (b) The difference and the standard deviation between measurement mean temperatures and controlled temperatures.

The comparison of sensing features between the demonstrated fiber laser temperature sensor and other WGM-based methods is listed in Table 1. Overall, the solid microcavity sensors have a better resolution than other reported sensors. On the contrary, the advantage of liquid and hybrid sensors is high sensitivity. Through FRL-enhanced and high thermo-optic coefficient liquid core, the proposed temperature sensor can achieve a relative high sensitivity and resolution at the same time. In the future, other materials with higher thermo-optic coefficient can be selected as the liquid core to further improve the sensitivity, such as cholesteric liquid crystal [12]. Furthermore, other WGM-based microcavities can be inserted as sensing unit into the FRL system for enhancement. The sensor package methods, such as designing

packaged structure to fix the position of each part [7, 27, 28] and implement an UV glue packaging technique to cover the coupling region [10], can be implemented to further improve the robustness and stability of the entire sensing unit for practical applications. The long distance remote sensing may be achieved by combining distributed Raman amplification in FRL system [29, 30]. The high OSNR is the most important parameter to achieve long distance, which is the advantage of our system. The sensing unit with ethanol core has been tested from 0 ℃ to 30 ℃ in fiber ring laser system, which covers the temperature range in upper mixed layer ocean applications [31], as shown in Fig. 8. Each time the temperature change is 3 ℃, and the acquisition was performed after waiting for one minute. The sensor temperature measurement range is limited to the material properties of the microtubule and the liquid core, especially the latter characteristic [13].

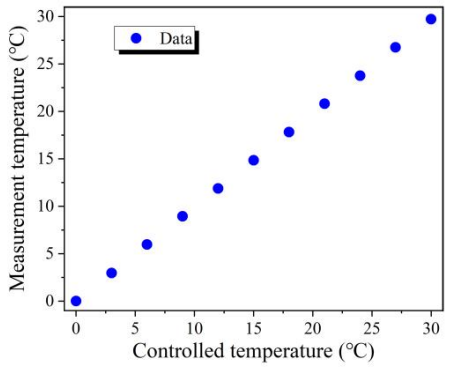

Fig. 8. The measurement temperatures of the sensing system with ethanol core microtubule.

TABLE I
COMPARISON OF SENSING FEATURES BETWEEN THE DEMONSTRATED FIBER LASER TEMPERATURE SENSOR AND OTHER WGM-BASED METHODS

State	Structure	Sensitivity (pm/°C)	Resolution (°C)	OSNR (dB)	Ref
Solid	Silica microsphere	13.37	1.1×10^{-3}	/	[10]
	Polymethylmethac-rylate microbubble	39	1.23×10^{-1} *	8	[16]
	Lithium niobate microdisk	6.67	8×10^{-4}	/	[32]
	PDMS microsphere	245	2×10^{-4}	/	[14]
Liquid	Dye-doped Oil Droplet	377	1.73×10^{-2} *	20	[11]
		112	2.7	/	[18]
	Dye-doped liquid crystal droplet	1500	3.07×10^{-2} *	/	[12]
	Liquid crystal microdroplet	267.6	7.5×10^{-2}	10	[19]
Hybrid	Liquid-core silica microbubble	200	8.5×10^{-3}	/	[13]
	Liquid-core silica microsphere	334.3	1.25×10^{-1} *	23	[33]
	FRL enhanced liquid-core silica microtubule	112.8	8.16×10^{-3}	52	Ours

* The calculation method is induced in Ref. [14], and the spectral resolution is considered as one-twentieth of the resonant peak FWHM. The calculation results were estimated according to the optimal data in the references.

IV. CONCLUSION

In summary, a high sensitivity and high resolution temperature sensing system based on the FRL enhanced WGM microtubule is demonstrated. The temperature response of thin wall thickness WGM microtubule is improved by injecting high thermo-optic coefficient liquid and its theoretical model is presented. A general method based on FRL is proposed for high resolution measurement and the WGM microtubule works as the sensing unit in the FRL. Due to the temperature characteristics of the microtubule, it is introduced into the fiber ring cavity as a temperature-tunable filter. So, the output sensing laser of the FRL has a high resolution to temperature. Experimental results show that the sensing laser has a linear blueshift when temperature increase. The sensitivity is as high as 112.8 pm/℃ and the resolution is 8.16×10^{-3} ℃. The proposed method can be extensible to WGM-based sensors and has a great potential in temperature sensing.

Uncategorized References

[1] D. K. Armani, T. J. Kippenberg, S. M. Spillane, and K. J. Vahala, "Ultra-high-Q toroid microcavity on a chip," *Nature,* vol. 421, no. 6926, pp. 925-8, Feb 27 2003

[2] B. Gayral, J. M. Gerard, A. Lemaitre, C. Dupuis, L. Manin, and J. L. Pelouard, "High-Q wet-etched GaAs microdisks containing InAs quantum boxes," (in English), *Appl Phys Lett,* vol. 75, no. 13, pp. 1908-1910, Sep 27 1999

[3] T. Ioppolo and M. V. Otugen, "Pressure tuning of whispering gallery mode resonators," (in English), *J Opt Soc Am B,* vol. 24, no. 10, pp. 2721-2726, Oct 2007

[4] P. Rabiei, W. H. Steier, C. Zhang, and L. R. Dalton, "Polymer micro-ring filters and modulators," (in English), *J Lightwave Technol,* vol. 20, no. 11, pp. 1968-1975, Nov 2002

[5] Y. Yang, S. Saurabh, J. M. Ward, and S. Nic Chormaic, "High-Q, ultrathin-walled microbubble resonator for aerostatic pressure sensing," *Opt Express,* vol. 24, no. 1, pp. 294-9, Jan 11 2016

[6] A. Bianchetti, A. Federico, S. Vincent, S. Subramanian, and F. Vollmer, "Refractometry-based air pressure sensing using glass microspheres as high-Q whispering-gallery mode microresonators," (in English), *Opt Commun,* vol. 394, pp. 152-156, Jul 1 2017

[7] V. Kavungal, G. Farrell, Q. Wu, A. K. Mallik, and Y. Semenova, "A Packaged Whispering Gallery Mode Strain Sensor Based on a Polymer-Wire Cylindrical Micro Resonator," (in English), *J Lightwave Technol,* vol. 36, no. 9, pp. 1757-1765, May 1 2018

[8] Y. J. Chen, U. Schoeler, C. B. Huang, and F. Vollmer, "Combining Whispering-Gallery Mode Optical Biosensors with Microfluidics for Real-Time Detection of Protein Secretion from Living Cells in Complex Media," *Small,* vol. 14, no. 22, p. e1703705, May 2018

[9] M. D. Baaske, M. R. Foreman, and F. Vollmer, "Single-molecule nucleic acid interactions monitored on a label-free microcavity biosensor platform," *Nat Nanotechnol,* vol. 9, no. 11, pp. 933-9, Nov 2014

[10] Y. Z. Yan *et al.*, "Packaged silica microsphere-taper coupling system for robust thermal sensing application," *Opt Express,* vol. 19, no. 7, pp. 5753-9, Mar 28 2011

[11] Z. Liu *et al.*, "Whispering gallery mode temperature sensor of liquid microresonastor," *Opt Lett,* vol. 41, no. 20, pp. 4649-4652, Oct 15 2016

[12] Y. Wang, H. Y. Li, L. Y. Zhao, Y. J. Liu, S. Q. Liu, and J. Yang, "Tunable whispering gallery modes lasing in dye-doped cholesteric liquid crystal microdroplets," (in English), *Appl Phys Lett,* vol. 109, no. 23, Dec 5 2016

[13] J. M. Ward, Y. Yang, and S. N. Chormaic, "Highly Sensitive Temperature Measurements With Liquid-Core Microbubble Resonators," (in English), *Ieee Photonic Tech L,* vol. 25, no. 23, pp. 2350-2353, Dec 1 2013

[14] C. H. Dong *et al.*, "Fabrication of high-Q polydimethylsiloxane optical microspheres for thermal sensing," *Appl Phys Lett,* vol. 94, no. 23, 2009

[15] T. Carmon, L. Yang, and K. Vahala, "Dynamical thermal behavior and thermal self-stability of microcavities," *Opt Express,* vol. 12, no. 20, pp. 4742-50, Oct 4 2004

[16] C. H. He *et al.*, "Temperature sensor based on high-Q polymethylmethacrylate optical microbubble," (in English), *Laser Phys,* vol. 28, no. 7, Jul 2018

[17] H. S. Chuang and S. Wereley, "Design, fabrication and characterization of a conducting PDMS for microheaters and temperature sensors," (in English), *J Micromech Microeng,* vol. 19, no. 4, Apr 2009

[18] R. Zeltner, R. Pennetta, S. Xie, and P. S. J. Russell, "Flying particle microlaser and temperature sensor in hollow-core photonic crystal fiber," *Opt Lett,* vol. 43, no. 7, pp. 1479-1482, Apr 1 2018

[19] Y. Wang, H. Li, L. Zhao, Y. Liu, S. Liu, and J. Yang, "Tapered optical fiber waveguide coupling to whispering gallery modes of liquid crystal microdroplet for thermal sensing application," *Opt Express,* vol. 25, no. 2, pp. 918-926, Jan 23 2017

[20] Z. Yu *et al.*, "Investigation of fused tapering with inner pressurized air for microcapillary-based optical sensor," (in English), *Opt Fiber Technol,* vol. 45, pp. 244-249, Nov 2018

[21] R. P. kenny, T. A. Birks, and K. P. Oakley, "Control of optical fibre taper shape," *Electronics Letters,* vol. 27, no. 18, 1991

[22] J. C. Knight, G. Cheung, F. Jacques, and T. A. Birks, "Phase-matched excitation of whispering-gallery-mode resonances by a fiber taper," *Opt Lett,* vol. 22, no. 15, pp. 1129-31, Aug 1 1997

[23] Z. Y. H. Wang *et al.*, "Ultra-sensitive DNAzyme-based optofluidic biosensor with liquid crystal-Au nanoparticle hybrid amplification for molecular detection," (in English), *Sensor Actuat B-Chem,* vol. 359, May 15 2022

[24] V. Zamora, A. Diez, M. V. Andres, and B. Gimeno, "Refractometric sensor based on whispering-gallery modes of thin capillarie," *Opt Express,* vol. 15, no. 19, pp. 12011-6, Sep 17 2007

[25] T. Ling and L. J. Guo, "A unique resonance mode observed in a prism-coupled micro-tube resonator sensor with superior index sensitivity," *Opt Express,* vol. 15, no. 25, pp. 17424-32, Dec 10 2007

[26] M. Chen, Z. Meng, J. Wang, and W. Chen, "Ultra-narrow linewidth measurement based on Voigt profile fitting," *Opt Express,* vol. 23, no. 5, pp. 6803-8, Mar 9 2015

[27] V. Kavungal, G. Farrell, Q. Wu, A. K. Mallik, and Y. Semenova, "Thermo-optic tuning of a packaged whispering gallery mode resonator filled with nematic liquid crystal," *Opt Express,* vol. 26, no. 7, pp. 8431-8442, Apr 2 2018

[28] J. Liao and L. Yang, "Optical whispering-gallery mode barcodes for high-precision and wide-range temperature measurements," *Light Sci Appl,* vol. 10, no. 1, p. 32, Feb 5 2021

[29] M. Fernandez-Vallejo, M. Bravo, and M. Lopez-Amo, "Ultra-Long Laser Systems for Remote Fiber Bragg Gratings Arrays Interrogation," (in English), *Ieee Photonic Tech L,* vol. 25, no. 14, pp. 1362-1364, Jul 15 2013

[30] M. Fernandez-Vallejo, M. Bravo, and M. Lopez-Amo, "200-km long fiber ring laser for multiplexing fiber Bragg gratings arrays," (in English), *Proc Spie,* vol. 8421, 2012

[31] N. Xu *et al.*, "Influence of temperature-salinity-depth structure of the upper-ocean on the frequency shift of Brillouin LiDAR," *Opt Express,* vol. 29, no. 22, pp. 36442-36452, Oct 25 2021

[32] R. Luo, H. Jiang, H. Liang, Y. Chen, and Q. Lin, "Self-referenced temperature sensing with a lithium niobate microdisk resonator," *Opt Lett,* vol. 42, no. 7, pp. 1281-1284, Apr 1 2017

[33] S. Liu *et al.*, "Whispering gallery modes in a liquid-filled hollow glass microsphere," *Opt Lett,* vol. 42, no. 22, pp. 4659-4662, Nov 15 2017